J Bioenerg Biomembr (2008) 40:245–255
DOI 10.1007/s10863-008-9154-x

Low resolution structure of subunit *b* ($b_{22–156}$) of *Escherichia coli* F_1F_O ATP synthase in solution and the *b*–δ assembly

Ragunathan Priya · Vikeramjeet S. Tadwal · Manfred W. Roessle · Shovanlal Gayen · Cornelia Hunke · Weng Chuan Peng · Jaume Torres · Gerhard Grüber

Received: 29 April 2008 / Accepted: 9 June 2008 / Published online: 31 July 2008

Abstract The first low resolution solution structure of the soluble domain of subunit *b* ($b_{22–156}$) of the *Escherichia coli* F_1F_O ATPsynthase was determined from small-angle X-ray scattering data. The dimeric protein has a boomerang-like shape with a total length of 16.2±0.3 nm. Fluorescence correlation spectroscopy (FCS) shows that the protein binds effectively to the subunit δ, confirming their described neighborhood. Using the recombinant C-terminal domain ($\delta_{91–177}$) of subunit δ and the C-terminal peptides of subunit *b*, $b_{120–140}$ and $b_{140–156}$, FCS titration experiments were performed to assign the segments involved in δ–*b* assembly. These data identify the very C-terminal tail $b_{140–156}$ to interact with $\delta_{91–177}$. The novel 3D structure of this peptide has been determined by NMR spectroscopy. The molecule adopts a stable helix formation in solution with a flexible tail between amino acid 140 to 145.

Keywords F_1F_O ATP synthase · F_1 ATPase · A_1A_O ATP synthase · Small angle X-ray scattering · Fluorescence correlation spectroscopy · NMR spectroscopy

R. Priya · V. S. Tadwal · S. Gayen · C. Hunke · W. C. Peng · J. Torres · G. Grüber (✉)
School of Biological Sciences,
Nanyang Technological University,
60 Nanyang Drive,
637551 Singapore, Singapore
e-mail: ggrueber@ntu.edu.sg

M. W. Roessle
Hamburg Outstation, European Molecular Biology Laboratory,
EMBL c/o DESY,
22603 Hamburg, Germany

Abbreviations

DSS	2,2-dimethyl-2-silapentane-5-sulfonate
DTT	dithiothreitol
EDC	1-ethyl-3-(dimethylaminopropyl)-carbodiimide
FCS	fluorescence correlation spectroscopy
HSQC	heteronuclear single quantum coherence
IPTG	isopropyl-β-D-thio-galactoside
NMR	nuclear magnetic resonance
NOESY	nuclear Overhauser effect spectroscopy
NTA	nitrilotriacetic acid
PAGE	polyacrylamide gel electrophoresis
PCR	polymerase chain reaction
SAXS	small angle X-ray scattering
SDS	sodium dodecyl sulfate
TFE	trifluorethanol
TOCSY	total correlation spectroscopy
Tris	Tris-(hydroxymethyl)aminomethane

Introduction

Adenosine 5′-triphosphate (ATP) synthesis by oxidative phosphorylation or photophosphorylation is a multistep membrane-located process that provides the bulk of cellular energy in eukaryotes and many prokaryotes. The majority of ATP synthesis is accomplished by the enzyme ATP synthase (EC 3.6.1.34) also called as F_1F_O ATP synthase, which, in its simplest form, as in bacteria, is composed of eight different subunits (α_3:β_3:γ:δ:ε:*a*:b_2:$c_{9–12}$). This multisubunit complex is divided into the F_1 headpiece, α_3:β_3, attached by a central and a peripheral stalk to a membrane-embedded ion-translocating part known as F_O. ATP is synthesized or hydrolyzed on the α_3:β_3 hexamer and the energy provided for or released during that process is

transmitted to the membrane-bound F_O sector, consisting of the subunits *a*, *c* and partially *b*. The energy coupling between the two active domains occurs via the stalk part (s) (Capaldi et al. 1996). The central stalk is made of subunit γ–ε, whereby the peripheral stalk is formed by the subunits δ and *b*, respectively. The peripheral stalk, which lies at the edge of the multi-subunit assembly of the F_1F_O ATP synthase acts as a stator to counter the tendency of the α_3:β_3 hexamer to follow the rotation of the central stalk and the attached *c*-ring, and to anchor the membrane-embedded *a* subunit (Pedersen et al. 2000; Weber 2006).

In *Escherichia coli*, structural features of subunit δ are available from the NMR derived solution model of the N-terminal domain (residues 1–134) of δ, suggesting a bundle of six α-helices forming a β-barrel (Wilkens et al. 1997). Subunit δ, with its 177 residues, is described to be linked with subunit *b* via their C-termini (Rodgers et al. 1997; McLachlin et al. 2000). Subunit *b* extends with its *soluble* part (b_{sol}) from the top of the F_1 sector down, into and across the membrane, where it is associated with subunit *a* (Weber 2006; Dunn et al. 2000; Bhatt et al. 2005; Altendorf et al. 2000). The 156 residue *b* subunit has been divided into four functional domains (Dunn et al. 2000). They are in order from C- to N-terminus, the δ-binding domain, the dimerization domain, the tether region and the membrane domain. The structure of the synthesized 34 residues long peptide of the N-terminal and partially membrane spanning region has been solved by ^{1}H NMR, showing an α helical feature (Dmitriev et al. 1999). Small angle X-ray scattering (SAXS) and analytical ultracentrifuge studies revealed that the segment $b_{62–122}$ is dimeric in solution, whereby the crystallographic model of the same peptide shows a monomeric α-helix with a length of 9.0 nm (Del Rizzo et al. 2002). The differences observed might be caused by the high concentration of hydrophobic solvents used in the crystallization conditions (Del Rizzo et al. 2002). So far no low or high resolution structure is available of the δ-binding- and tether domain or the entire soluble part of subunit *b* (b_{sol}), including the δ-binding-, dimerization domain, and tether region, which extends from the membrane up to the top of the catalytic $\alpha_3\beta_3$ hexamer. Another issue concerning the peripheral stalk subunit *b* is its specific association with the C-terminus of subunit δ.

Here, we have turned our attention to the examination of b_{sol} (residues 22–156) of the *E. coli* F_1F_O ATP synthase (*EC*F_1F_O ATP synthase) and describe the structural features of this stalk subunit in solution using SAXS. Fluorescence correlation spectroscopy (FCS) has been performed to map the segments of δ–*b* assembly. Finally, the solution structure of the C-terminal helix, involved in such association, is solved by NMR spectroscopy.

Experimental procedures

Biochemicals

ProofStart™ DNA Polymerase and Ni^{2+}-NTA-chromatography resin were received from Qiagen (Hilden, Germany); restriction enzymes were purchased from Fermentas (St. Leon-Rot, Germany). Chemicals for gel electrophoresis were received from Serva (Heidelberg, Germany). Bovine serum albumin was purchased from GERBU Biochemicals (Heidelberg, Germany). $(^{15}NH_4)_2SO_4$ was purchased from Cambridge Isotope Laboratories (Andover, USA). All other chemicals were at least of analytical grade and received from BIOMOL (Hamburg, Germany), Merck (Darmstadt, Germany), Roth (Karlsruhe, Germany), Sigma (Deisenhofen, Germany), or Serva (Heidelberg, Germany).

Production and purification of proteins

To amplify the soluble domain of *atpF* gene ($b_{21–156}$ and $b_{22–156}$), oligonucleotide primers 5′-CCT GTT CA*C CAT GG*C TTG CA-3′ (forward primer) for $b_{21–156}$ and 5′-CCT GTT CA*C CAT GG*C TTG CA-3′ (forward primer) for $b_{22–156}$ and the same reverse primer 5′ CCC *GAG CTC* CTT ACA GTT CAG 3′ for both the constructs, incorporating *Nco*I and *Sac*I restriction sites (italic), were designed. In order to amplify *atp*H gene for subunit δ and the truncated form $\delta_{91–177}$, oligonucleotide primers 5′-T*CC ATG G*CT ATG TCT GAA TTT ATT ACG GTA G-3′ (forward primer) and 5′-TTT T*CC ATG G*CT GAT GTT CTG GAG-3′ (forward primer), respectively, and the same reverse primer 5′-TTC *GAG CTC* TTA AGA CTG CAA GAC GTC-3′ for both the constructs, incorporating *NcoI* and *SacI* restriction sites (underlined), were designed. The *unc* containing plasmid pGG1 (Grüber et al. 1997) was used as the template for polymerase chain reaction (PCR). Following digestion with *Nco*I and *Sac*I, the PCR products were ligated into the pET9d1-His_3 vector. The pET9d1-His_3 vector, containing the soluble portions of gene *atp*F and *atp*H, was then transformed into *E. coli* cells (strain BL21 (DE3)) and grown on 30 μg/ml kanamycin-containing Luria–Bertoni (LB) agar-plates. To produce the proteins, liquid cultures were shaken in LB medium containing kanamycin (30 μg ml^{-1}) for about 6 h at 37 °C until an optical density OD_{600} of 0.6–0.7 was reached. To induce the production of His_3–$b_{21–156}$–δ, –$b_{22–156}$–δ, –δ or $\delta_{91–177}$ the cultures were supplemented with isopropyl (thio)-β-D-galactoside (IPTG) to a final concentration of 1 mM. Following incubation for another 4 h at 30 °C, the cells were harvested at 10,000×*g* for 15 min, 4 °C. Subsequently, they were lysed on ice by sonication for 3×1 min in appropriate buffers, $b_{21–156}$–δ and $b_{22–156}$–δ in buffer A (50 mM Tris/HCl, pH 9.0,

200 mM NaCl, 1 mM DTT, 1 mM PMSF), subunit δ in buffer B (50 mM Tris/HCl, pH 9.0, 200 mM NaCl, 0.8 mM DTT, 1 mM PMSF) and δ_{91-177} in buffer C (50 mM Tris/HCl, pH 7.5, 200 mM NaCl, 0.8 mM DTT, 1 mM PMSF). The lysate was cleared by centrifugation at 10,000×*g* for 35 min. The supernatant was filtered (0.45 μm; Millipore) and passed over a 2 ml Ni^{2+}-NTA resin column to isolate the proteins, respectively, according to (Grüber et al. 2002). The His-tagged protein was allowed to bind to the matrix for 2 h at 4 °C and eluted with an imidazole-gradient (25–300 mM) in buffer A, B, C, respectively. Fractions containing His_3-tagged were identified by SDS-PAGE (Laemmli 1970) pooled and concentrated as required using centricon YM-3 or YM-5 (3 and 5 kDa molecular mass cut off) spin concentrators (Millipore). Imidazole was removed by gel filtration chromatography using a Superdex 75 HR 10/30 column (GE Healthcare) and a buffer of 50 mM Tris/HCl (pH 9.0) and 200 mM NaCl for b_{21-156} and b_{22-156} and δ. In the case of δ_{91-177} imidazole was removed by HiTrap desalting column (GE Healthcare) and a buffer of 50 mM Tris, pH 7.5, 200 mM NaCl.

The purity and homogeneity of all protein samples were analyzed by SDS-PAGE (Laemmli 1970). SDS-gels were stained with Coomassie Brilliant Blue G250. Protein concentrations were determined by the bicinchoninic acid assay (BCA; Pierce, Rockford, IL, USA).

Peptide synthesis

The peptides $b_{120-140}$ and $b_{140-156}$ were synthesized on Liberty Automatic Microwave Peptide Synthesizer (CEM, USA) using *N*-(9-fluorenyl) methoxycarbonyl (Fmoc) chemistry on a Rink amide MBHA resin (Novabiochem, Germany). The C-terminal amidated peptides were purified by reverse-phase high performance liquid chromatography (HPLC) on a Dynamax C-18 column (Varian Inc., USA) eluted with a linear 5–100% gradient of acetonitrile in 0.04% aqueous trifluoroacetic acid. The identity of the purified peptide was confirmed by MALDI-TOF mass spectrometry (4800 MALDI TOF/TOF, AB Applied Biosystems MDS Sciex, USA). The purity of the peptides was confirmed by electrospray ionization (ESI) mass spectrometry.

Circular dichroism spectroscopy

Steady state circular dichroism (CD) spectra were measured in the far UV-light (185–260 nm) using a CHIRASCAN spectropolarimeter (Applied Photophysics). Spectra were collected in a 60 μl quartz cell (Hellma) with a path length of 0.1 mm, at 20 °C and a step resolution of 1 nm. The readings were average of 2 s at each wavelength and the recorded ellipticity values were the average of three determinations for each sample. CD spectroscopy of b_{22-156} (2.0 mg/ml) was performed in respective buffer. The spectrum for the buffer was subtracted from the spectrum of the protein. CD values were converted to mean residue ellipticity (Θ) in units of degree cm^2 $dmol^{-1}$ using the software *Chirascan Version 1.2*, Applied Photophysics. This baseline corrected spectrum was used as input for computer methods to obtain predictions of secondary structure. In order to analyze the CD spectrum the following algorithms were used: Varselec (Manavalan and Johnson 1987), Selcon (Sreerama and Woody 1993), Contin (Provencher 1982), K2D (Andrade et al. 1993) (all methods as incorporated into the program Dicroprot (Deléage and Geourjon 1993) and NeuralNet (Böhm 1992)).

X-ray scattering experiments and data analysis

The synchrotron radiation X-ray scattering data were collected following standard procedures on the X33 SAXS camera (Boulin et al. 1986; Boulin et al. 1988) of the EMBL Hamburg located on a bending magnet (sector D) on the storage ring DORIS III of the Deutsches Elektronen Synchrotron (DESY). As detector, a single photon counting pixel detector system (PILATUS 500k) was used. A sample–detector distance of 2,675 mm was used, covering the range of momentum transfer $0.1<s<5$ nm^{-1} ($s = 4\pi \sin(\theta)/\lambda$, where θ is the scattering angle and $\lambda = 0.1504$ nm is the X-ray wavelength). The *s*-axis was calibrated by the scattering pattern of Silver-behenate salt (*d*-spacing 5.84 nm). The scattering patterns from b_{22-156} protein was measured at protein concentrations of 3.0 and 8.0 mg/ml. Protein sample was prepared in 50 mM Tris/HCl (pH 9.0), 200 mM NaCl and 1 mM DTT as radical quencher. Four repetitive measurements of 30 s at 15 °C of the same protein solution were performed in order to check for radiation damage. Stable intensities especially at low angles indicated that no protein aggregation take place during the exposure times. After radial averaging the data were normalized to the intensity of the incident beam; the scattering of the buffer was subtracted and the difference curves were scaled for concentration. A final data set was merged from the data recorded at different concentrations and the lower concentration data was taken at lower *s* values. All the data processing steps were performed automatically using the program packages AutoPILATUS, AutoSUB and PRIMUS (Konarev et al. 2003; Petoukhov et al. 2007). The forward scattering $I(0)$ and the radius of gyration R_g were evaluated using the Guinier approximation (Guinier and Fournet 1955) by the AutoRG (Petoukhov et al. 2007) assuming that for spherical particles at

very small angles ($s<1.3/R_g$) the intensity is represented by $I(s) = I(0)\exp(-(sR_g)^2/3)$. These parameters were also computed from the entire scattering patterns using the indirect transform package GNOM (Svergun 1993), which also provide the distance distribution function $p(r)$ of the particle as defined:

$$p(r) = 2\pi \int I(s)\, sr\, \sin(sr)\, \mathrm{d}s$$

The molecular mass of $b_{22–156}$ was calculated by comparison with the forward scattering from the reference solution of bovine serum albumin (BSA). From this procedure a relative calibration factor for the molecular mass (MM) can be calculated using the known molecular mass of BSA (66 kDa) and the concentration of the reference solution by applying

$$MM_p = I(0)_p / c_p \times \frac{MM_{st}}{I(0)_{st}/c_{st}}$$

where $I(0)_p$, $I(0)_{st}$ are the scattering intensities at zero angle of the studied and the BSA standard protein, respectively, MM_p, MM_{st} are the corresponding molecular masses and c_p, c_{st} are the concentrations. Errors have been calculated from the upper and the lower $I(0)$ error limit estimated by the Guinier approximation.

Low-resolution models of $b_{22–156}$ was built by the program DAMMIN (Svergun 1992), which represents the protein as an assembly of dummy atoms inside a search volume defined by a sphere of the diameter D_{max}. Starting from a random model, DAMMIN employs simulated annealing to build a scattering equivalent model fitting the experimental data $I_{exp}(s)$ to minimize discrepancy:

$$\chi^2 = \frac{1}{N-1}\sum_j \left[\frac{I_{exp}(s_j) - cI_{calc}(s_j)}{\sigma(s_j)}\right]^2$$

where N is the number of experimental points, c a scaling factor and $I_{calc}(s_j)$ and $\sigma(s_j)$ are the calculated intensity and the experimental error at the momentum transfer s_j, respectively. Ab initio shape models for $b_{22–156}$ was obtained by superposition of ten independent DAMMIN reconstructions for each subunit by using the program packages DAMAVER (Svergun 1997) and SUBCOMP (Svergun et al. 2001).

NMR data collection and processing

Peptide $b_{140–156}$ was prepared by dissolving appropriate amount in 25 mM phosphate buffer pH 6.8 and 30% TFE-d3. The one dimensional (1D) and two dimensional (2D) ^{1}H NMR spectra including total correlation spectroscopy (TOCSY) and nuclear overhauser enhancement spectroscopy (NOESY) were obtained at the temperature of 288 K on a Avance Bruker NMR spectrometer at 600 MHz proton frequency. TOCSY and NOESY spectra of the peptide were recorded with mixing times of 80 and 300 ms, respectively. All the NMR data were processed using Bruker Advance spectrometer in-built software Topspin. Peak-picking and data analysis of the Fourier-transformed spectra were performed with SPARKY program (Kneller and Goddard 1997). Assignments were carried out according to classical procedures including spin-system identification and sequential assignment (Wüthrich 1986).

Structure calculation

Three-dimensional structure of peptide $b_{140–156}$ was calculated based on both distance and angle restraints by using CYANA 2.1 program package (Herrmann et al. 2002). Dihedral angle restraints were calculated from chemical shifts using torsion angle likelihood obtained from shift and sequence similarity (TALOS) (Wüthrich 1986). In total 100 structures were calculated. An ensemble of 20 structures with lowest total energy was chosen for structural analysis. This final ensemble of accepted structures satisfies the following criteria: no NOE violations greater than 0.3 Å, r. m.s.d. of 0.491±0.31 Å.

Fluorescence correlation spectroscopy

Fluorescence correlation spectroscopy (FCS) has been performed on a ConfoCor 3 LSM-FCS system (Zeiss, Jena/Germany). To study the binding of $b_{22–156}$ to δ, subunit δ was labeled by incubating the protein with Atto488 maleimide for 10 min in 50 mM Tris, pH 9.0. The binding of the peptides $b_{120–140}$ and $b_{140–156}$ with $\delta_{91–177}$, respectively was analyzed, in which the peptide was labeled by the Atto655-NHS ester (*ATTO-TEC*, Siegen/Germany). The labeling was performed in 25 mM sodium phosphate buffer, pH 6.8 for 10 min. at room temperature. The excess of the unbound dye was removed using a ZipTip® P-10 Pipette Tip with C4 resin (Millipore, USA) by replacing the solution with 5% acetonitrile/water for seven times.

The 633 nm laser line of 5 mW HeNe laser for Atto655 labeled subunit *b* peptides and 488 nm laser line of 30 mW Ar-laser for Atto488 labeled subunit δ was focused into the aqueous solution by a water immersion objective (40×/1.2 W Corr UV-VIS-IR, Zeiss). FCS was measured in 15 µl droplets, which were placed on gelatin treated Lab-Tek™ eight well chambered cover glass according to Hunke et al. (2007). The following filter sets were used for Atto655: MBS: HFT 514/633, EF: None, DBS: None, EF2: BP 655-710 IR and for Atto488: MBS: HFT 488, EF: None, DBS: Mirror, EF2: LP 505. Out-of-focus fluorescence was rejected by a 90 µm pinhole in the detection pathway,

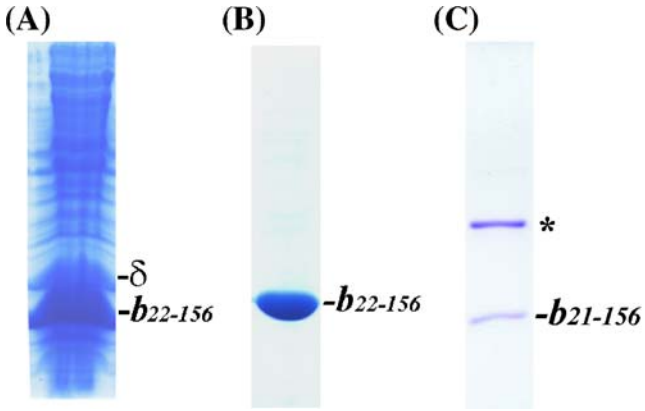

Fig. 1 An SDS-PAGE (17% total acrylamide and 0.4% crosslinked acrylamide) of recombinant expressed and purified $b_{22–156}$ (**a**, **b**) and purified $b_{21–156}$ (**c**) of F_1F_O ATP synthase from *E. coli*. *E. coli* BL21 cells, containing pET9d1–His_3–$b_{22–156}$–δ were induced by IPTG and the lysate was applied onto an SDS-PAGE (**a**). **b** shows the purified recombinant $b_{22–156}$. *Asterisk*, in **c** indicates the dimer formation of $b_{21–156}$

resulting in a confocal detection volume dimensions of L: 1.5 μm and Ø 0.3 μm. Fluorescence autocorrelation functions were measured for 30 s each with 12 repetitions in respective buffers. Solutions of fluorescent dyes Atto655, Atto488 and Cy5 in appropriate buffers were used as references for the calibration of the ConfoCor 3 beam path.

To analyze the autocorrelation functions of $b_{120–140}$ and $b_{140–156}$ bound to subunit $\delta_{91–177}$, respectively, a standard autocorrelation two diffusion coefficients normalized triplet model (FCS-LSM software, ConfoCor 3, Zeiss) was used for fitting. The diffusion time of fluorescently labeled peptides $b_{120–140}$ and $b_{140–156}$ was measured independently, and was kept fixed during the fitting of the FCS data. Therefore, the binding constants were determined by calculating the relative amount of free labeled $b_{140–156}$ that displays a shorter diffusion time in comparison with $\delta_{91–177}$ bound to $b_{140–156}$ with longer diffusion times. The calculations were done by the ConfoCor 3-software 4.2, Microsoft Excel 2003, and Origin 7.5.

Results

Production and purification of $b_{21–156}$ and $b_{22–156}$

Analysis of the nucleotide sequence of the *atp* operon of *E. coli* revealed that the gene encoding subunit *b*, *atp*F, and subunit δ, *atp*H, respectively, are connected via a Shine-Dalgarno sequence. This arrangement is also found in other prokaryotic systems, and suggests translational coupling between these genes, which may be important during translation and/or assembly of the F_1F_O complex (Brusilow et al. 1989; Keis et al. 2004). Two constructs were designed; one carries the DNA-sequence encoding for $b_{21–156}$ plus subunit δ ($b_{21–156}$–δ) and the second one consists of the DNA sequence for the production of $b_{22–156}$ plus subunit δ ($b_{22–156}$–δ). The SDS-PAGE of the produced recombinant $b_{21–156}$–δ revealed two prominent bands of 12 kDa ($b_{21–156}$) and 22 kDa (δ) which were found in crude lysates following IPTG induction. Similarly two bands with an apparent mass of 12 kDa ($b_{22–156}$) and 22 kDa (δ) in the ratio of about 2:1 were observed for the construct $b_{22–156}$–δ (Fig. 1a). A Ni^{2+}-NTA resin column and an imidazole-gradient (25–250 mM) in buffer consisting of 50 mM Tris/HCl (pH 9.0) and 200 mM NaCl was used to separate $b_{21–156}$–δ and $b_{22–156}$–δ, respectively, from the main contaminating proteins. Both, $b_{21–156}$–δ and $b_{22–156}$–δ, respectively, were subsequently applied to a Superdex 75 column, to separate the soluble *b* domain from subunit δ. Analysis of the isolated protein by SDS-PAGE revealed the high purity of the proteins $b_{21–156}$ and $b_{22–156}$ (Fig. 1). As demonstrated in Fig. 1c, $b_{21–156}$, positions 21 and 21′ of the first and second helix, respectively, are close including Cys_{21} forms a dimer in the absence of an oxidizing agent.

Circular dichroism spectra of $b_{21–156}$ and $b_{22–156}$

The secondary structure of $b_{22–156}$ was determined from circular dichroism spectra, measured between 185–260 nm (Fig. 2). The minima at 222 and 208 nm and the maximum at 192 nm indicate the presence of α-helical structures in the protein. The secondary structure content of the protein was calculated to be 77±2% α-helix. This result is consistent with secondary structure predictions based on subunit *b* amino-acid sequence. The molar ellipticity values at 208 and at 222 nm are in a ratio of 0.88.

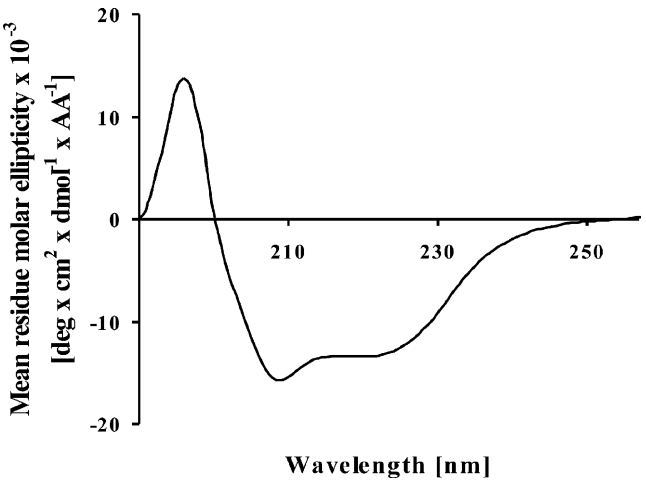

Fig. 2 Far UV-CD spectrum of $b_{22–156}$

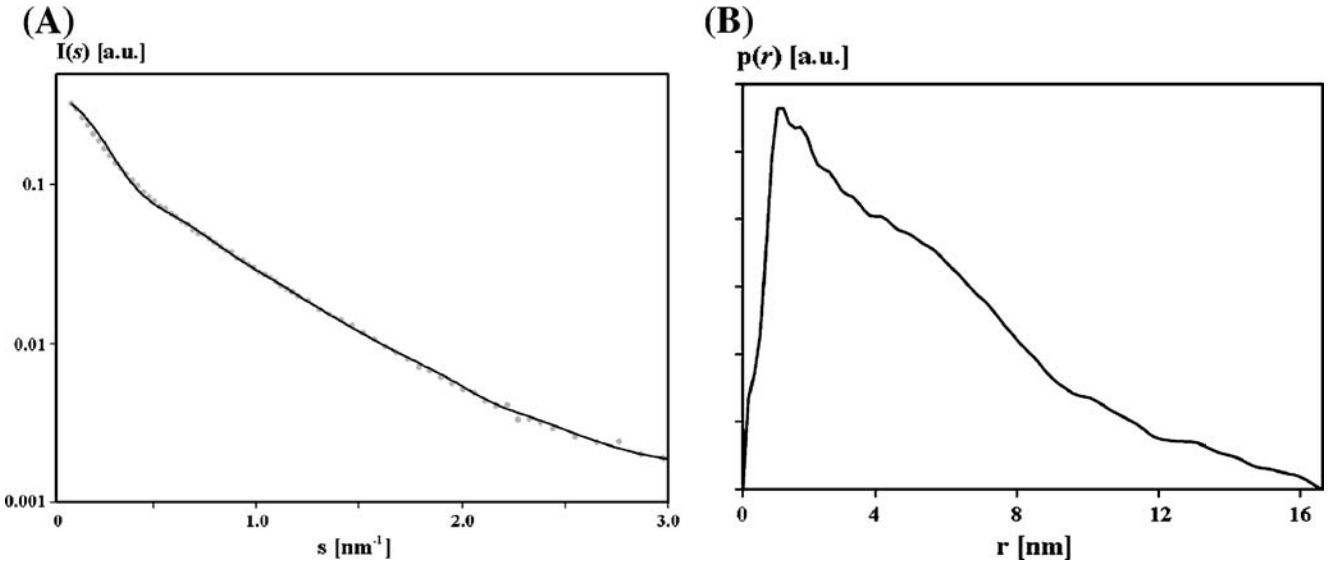

Fig. 3 **a** Experimental scattering curves (*dots*) and result from typical ab initio model of $b_{22–156}$ (*solid line*) computed by the program DAMMIN. **b** Distance distribution functions of $b_{22–156}$

Solution X-ray scattering experiments

X-ray solution scattering patterns of solutions of $b_{22–156}$ were recorded (Fig. 3a). The radius of gyration (R_g) of $b_{22–156}$ is found to be 3.42±0.07 nm and its maximum dimension (D_{max}) is 16.2±0.3 nm as deduced from a Guinier plot and from the distance distribution function $p(r)$ (Fig. 3b), calculated with the GNOM program (Guinier and Fournet 1955). Comparison of the forward scattering with the values obtained from a reference solution of bovine serum albumin, (BSA; 66±2 kDa) yields a molecular mass of 28±2 kDa, independently of the concentration used (3 and 8 mg/ml).

Shape and domain structure of $b_{22–156}$

The gross structure of $b_{22–156}$ was restored ab initio from the scattering patterns in Fig. 3a using the shape determination program DAMMIN as described in "Methods". The obtained shape for $b_{22–156}$ yields a good fit to the experimental data in the entire scattering range. The corresponding fit, shown in Fig. 3a, has a discrepancies of χ=3.1. All ten independent reconstructions yielded a reproducible shape and have been averaged (Fig. 4). $b_{22–156}$ appears as boomerang shaped molecule of two distinct parts.

Fluorescence correlation spectroscopy experiments

As subunit *b* has been shown to bind to subunit δ (Rodgers et al. 1997; McLachlin et al. 2000), the binding capacity of $b_{22–156}$ to δ has been confirmed by fluorescence correlation spectroscopy (FCS), in which subunit δ has been labeled with Atto488. A mean count rate of 38.8 kHz was determined for Atto488-δ as a reference. Fitting the autocorrelation functions resulted in a characteristic diffusion time of 243.0 μs for Atto655 labeled δ. Figure 5a displays

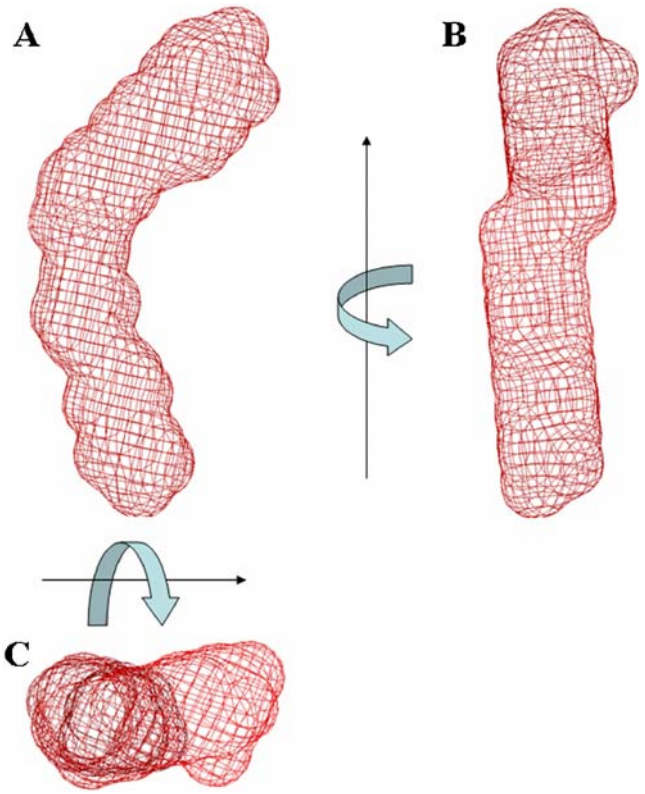

Fig. 4 Low resolution structure of $b_{22–156}$ determined from SAXS data. **b** Model **a** rotated by 90° around the *Y*-axis. **c**, model **a** rotated 90° around the *X*-axis. The mesh shape was generated by an advanced RASMOL version (Jemilawon et al. 2007)

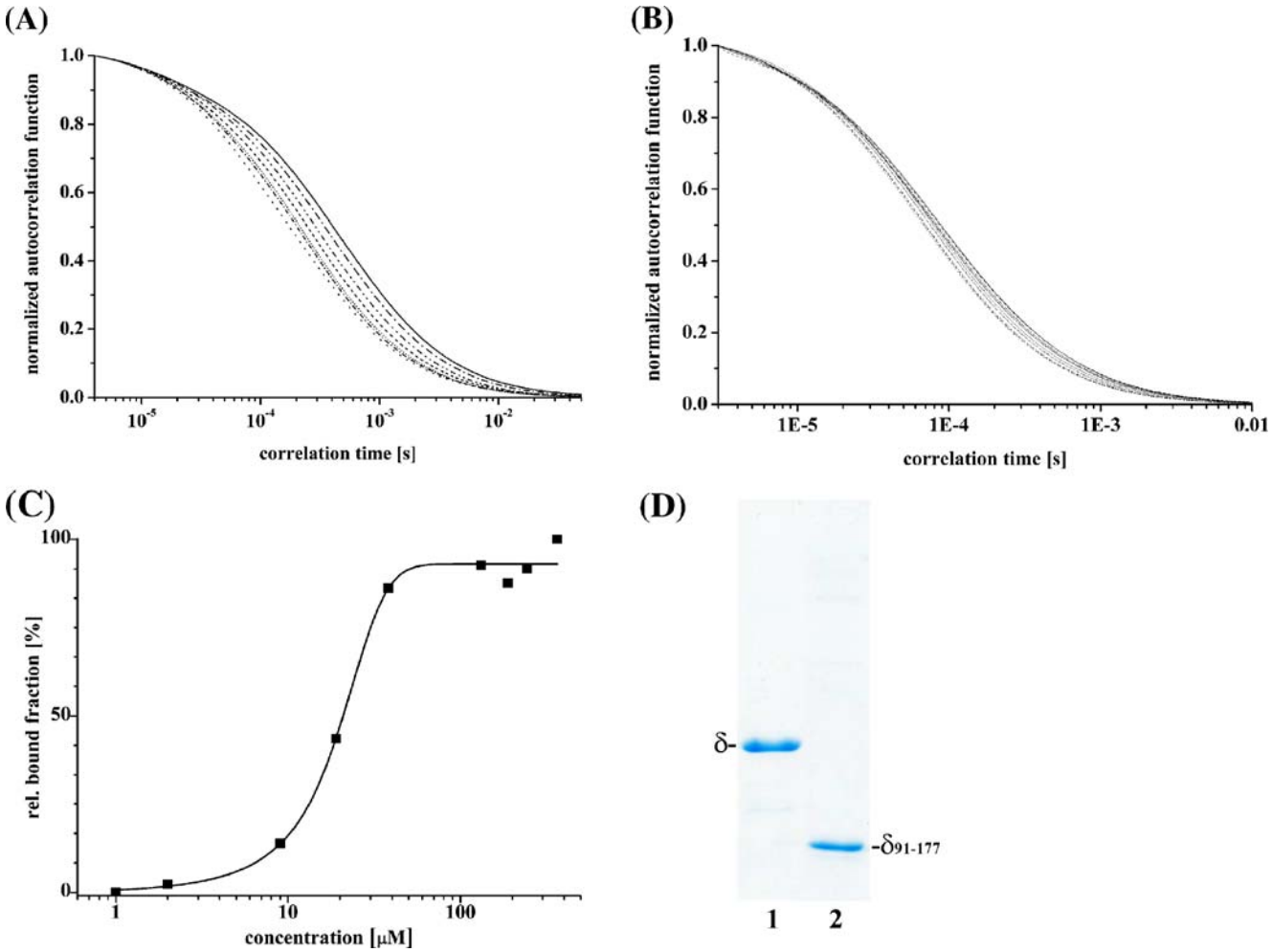

Fig. 5 Fluorescence correlation spectroscopy studies. **a** Normalized autocorrelation functions of Atto488 labeled subunit δ by increasing the quantity of $b_{22–156}$. **b** Normalized autocorrelation functions of Atto655–$b_{140–156}$ in the absence and presence of different concentrations of $\delta_{91–177}$. **c** Concentration-dependent binding of $b_{140–156}$ to $\delta_{91–177}$. The binding constant was calculated by determining the relative bound fraction using a standard autocorrelation two diffusion coefficients normalized triplet model (FCS-LSM software, ConfoCor 3, Zeiss). Best fits yielding the binding constants are represented as fitted line by a non-linear, Boltzmann curve fit (see the text). **d** An SDS-PAGE of recombinant expressed subunit δ (*lane 1*), and truncated $\delta_{91–177}$ (*lane 2*) of *EC*F_1F_O ATP synthase

the measured autocorrelation curves of the fluorescent labeled subunit δ in the absence and presence of $b_{22–156}$. The addition of protein caused in a significant change in the mean diffusion time, which went up with increasing concentrations of segment $b_{22–156}$. The increase in the diffusion time was due to the increase in the mass of the diffusing particle, as Atto488–δ was interacting with $b_{22–156}$, demonstrating the binding properties of the recombinant $b_{22–156}$. More recently, it has been proposed that subunit *b* might associate via its C-terminal region, including amino acids 120 to 156, with the C-terminus of subunit δ (Rodgers et al. 1997; McLachlin et al. 2000). In order to map the residues involved in *b*–δ formation, we synthesized the peptides $b_{120–140}$ and $b_{140–156}$, respectively, and isolated the recombinant C-terminal form $\delta_{91–177}$ (Fig. 5d). FCS experiments have been performed, in which $b_{140–156}$ has been labeled with Atto655–NHS ester. A mean count rate of 7.0 kHz was determined for Atto655–$b_{140–156}$ as a reference. Fitting the autocorrelation functions resulted in a characteristic diffusion time of 55.9 μs for Atto655 labeled $b_{140–156}$. Figure 5b displays the measured autocorrelation curves of the fluorescent labeled peptide $b_{140–156}$ in the absence and presence of $\delta_{91–177}$. The addition of protein caused in a significant change in the mean diffusion time, which went up with increasing concentrations of segment $\delta_{91–177}$, showing that the peptide $b_{140–156}$ interacts with the C-terminal domain of subunit δ. A binding constant of 18 μM of bound Atto655–$b_{140–156}$ to $\delta_{91–177}$ was calculated (Fig. 5c). On contrary, no binding of $\delta_{91–177}$ could be observed when labeled $b_{120–140}$ has been used in the experiments.

Assignment and structure calculation

To better understand the feature of the binding peptide $b_{140–156}$, we determined its 3D structure by NMR spectroscopy. Using the standard procedure for sequential assignment based on homonuclear TOCSY and NOESY experiments, all the residues of $b_{140–156}$ were assigned (Fig. 6a). The connectivity diagram of $b_{140–156}$ is indicative of a helical conformation with the sequential HN–HN, Hα–HN(i, $i+3$), Hα–HN(i, $i+4$), and Hα–Hβ(i, $i+3$) connectivities (Fig. 6b). Figure 7a shows an overlay of the twenty lowest energy structures of $b_{140–156}$, which have an overall root mean square deviation (RMSD) of 0.491±0.31. All these structures have energies lower than −100 kcal mol^{-1}, no NOE violations greater than 0.3 Å and no dihedral violations greater than 5°. The statistics are given in Table 1. The peptide displays a short flexible N-terminal tail of the amino acids 140 to 145 and helix structural motif formed by the residues 146 to 156 (Fig. 7a). The peptide exhibits amphiphilic character such that the negative charge spread on one side from the N- to the C-terminal end of the structure (Fig. 7b) while the positive charge (Fig. 7c) and a hydrophobic surface (Fig. 7d) form sides of the helix region.

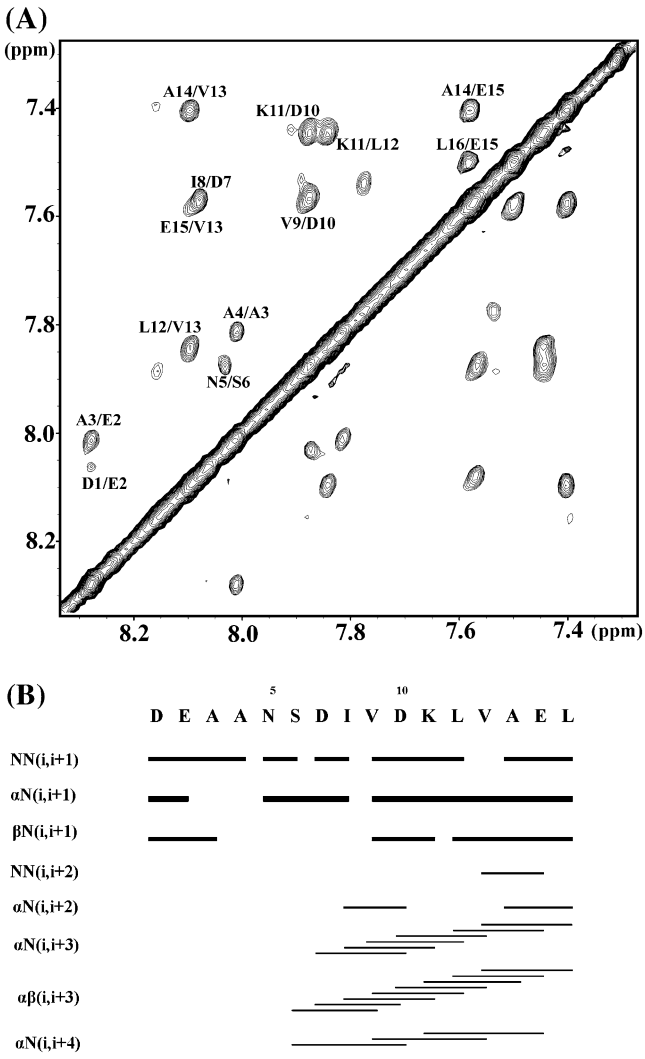

Fig. 6 **a** HN–HN region of the NOESY spectra of $b_{140–156}$. **b** Connectivity diagram of $b_{140–156}$. The *line thickness* reflects the intensities of the NOE connectivities

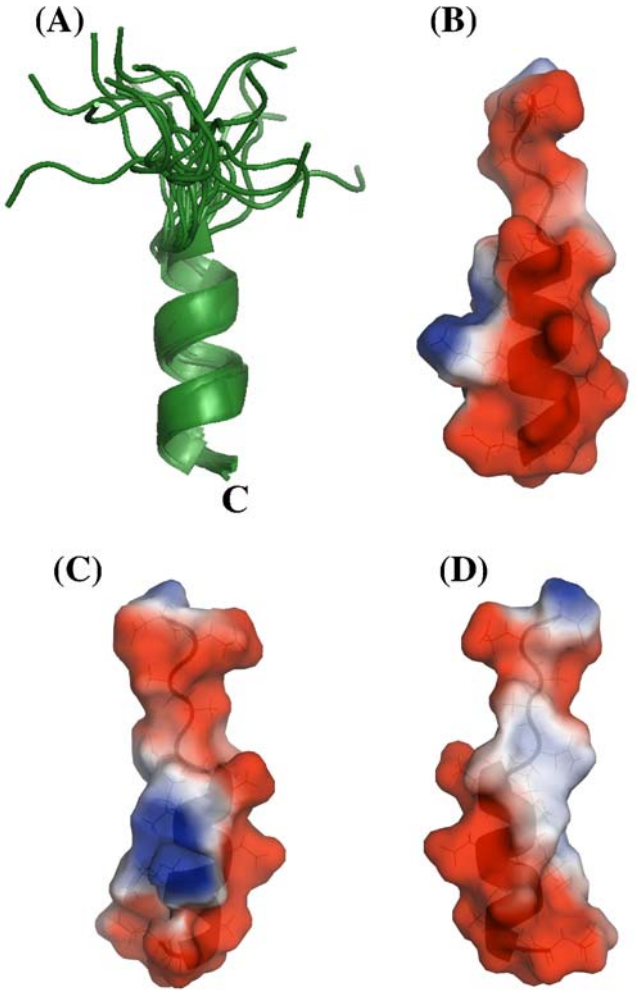

Fig. 7 Cartoon representation for the NMR structure of the peptide $b_{140–156}$. **a** Superposition of the twenty lowest energy structures. **b–d** Different orientations of $b_{140–156}$, showing the molecular surface with the electrostatic potential of the peptide, drawn in pyMol (53) that uses Poisson–Boltzmann equation, where the positive potentials are drawn in *blue* and negative in *red*

Discussion

The goal of this work was to express efficiently the soluble part of the peripheral stalk subunit b ($b_{22–156}$) of the $EC F_1F_O$ ATP synthase to yield pure and monodispersed protein retaining the first low resolution solution structure of this domain, which is predicted from its amino acid

Table 1 Structural statistics for $b_{140–156}$

Statistics	Value
Distance restraints	
Total	121
Intraresidue ($I-j=0$)	38
Sequential ($\|i-j\|=1$)	50
Medium-range ($2\leq\|i-j\|\leq4$)	30
Long-range ($\|i-j\|\geq5$)	0
Average number of violations	
Distance violations >5 Å	0
Ramachandran plot[2] (%)	
Residues in most favoured regions	63.9
Residues in additionally allowed regions	35.0
Residues in generously allowed regions	1.1
Residues in disallowed regions	0.0
Average RMSD to Mean (Å)	
Backbone (C^{α}, C′, and N)	0.491±0.31

sequence to be α-helical and has a high propensity to form a dimer (Fig. 3). The CD spectrum of $b_{22–156}$ is consistent with the predicted high helical content of this protein (77%), and also with an intermediate degree of coiling based on the $\Theta_{222}/\Theta_{208}$ ratio of 0.88. CD spectra of the truncated form $b_{53–124}$ showed that the coiled-coil interaction is mainly located in the segment of residues 30 to 122 (Revington et al. 2002). Physical characterization of this protein by small angle X-ray scattering supports unequivocally that $b_{22–156}$ is dimeric in solution (28±2 kDa), consistent with analytical ultracentrifugation data of the *b* subunit form $b_{21–156}$ (Del Rizzo et al. 2002). The X-ray data also yield a maximum dimension of 16.2±0.3 nm, indicating that $b_{22–156}$ is an elongated dimer. Both, the dimeric and elongated feature of $b_{22–156}$ are in line with SAXS-data of the peptide $b_{62–122}$, determined to be a dimer in solution of approximately 9.5 nm in length (Del Rizzo et al. 2002). Furthermore, the data presented explain, that the monomeric α-helical structure, determined from crystallographic data, might be due to the use of crystallization conditions, interrupting interactions of nonpolar core residues and thereby the coiled-coil formation (Del Rizzo et al. 2002). Whether both helices are oriented as left-handed (Hornung et al. 2008; Wise and Vogel 2008) or right-handed coiled coils, in which one of the helices is shifted relative to each other by 5.5 amino acids (Del Rizzo et al. 2006; Wood and Dunn 2007) is a matter of debate. At the resolution presented, we do not see an offset at the ends of the shape, which one might expect, if both helices are shifted by 5.5 residues. The high yield of disulfide formation of the native Cys_{21} and $Cys_{21'}$ residues in $b_{21–156}$ in the absence of any oxidizing reagent (Fig. 1c), imply that both helices are in a parallel and in-register arrangement, supporting most recent data, derived from electron spin resonance spectroscopy (ESR; Hornung et al. 2008) and simulated annealing modeling (Wise and Vogel 2008).

The novel low resolution structure of $b_{22–156}$ is similar concerning its length, curvature and shape to the density visible in some projection of the $EC F_1F_O$ ATP synthase, derived from negatively stained electron micrographs (Wilkens 2000). The observed boomerang-like conformation of $b_{22–156}$ resembles the curved form of the crystallographic model of the soluble domain (residues 79–184) subunit of the mitochondrial F_1F_O ATP synthase, which is about 16 nm long (Dickson et al. 2006). This monomeric *b* subunit interacts with subunit *d* via a parallel and two antiparallel coiled coil formation as well as with the C-terminal helix of subunit F6 (Dickson et al. 2006). In addition, the shape of $b_{22–156}$ enables the comparison to the homologue subunit H of the related A_1A_O ATP synthase. Subunit H forms also a homodimer of two α-helices with 20 nm in length, arranged in a parallel, in-register and coiled coil formation (Biuković et al. 2007). The $\Theta_{222}/\Theta_{208}$ ratio of subunit H (0.96) indicates that the two helices in subunit H form a stronger coiled-coil conformation (Biuković et al. 2007), compared to the ones in $b_{22–156}$ (0.88).

The structure of the F_1F_O ATP synthase from *E. coli* can be divided into four subregions, an F_1 headpiece, one peripheral- and central stalk-region, and the membrane embedded F_O part. The $EC F_1$ ATPase in solution has a maximum length of about 15 nm made-up by the F_1 headpiece (10.8 nm) and the central stalk (γ–ε), with about 4.2 nm in length (Grüber 2000; Hausrath et al. 1999). A maximum length of about 16 nm of the hydrated dimeric $b_{22–156}$ would exceed the total distance of about 15 nm, including the height of the central stalk and the F_1 headpiece. Previous studies have shown that subunit *b* is anchored inside the enzyme to subunit *a* via its N-terminal

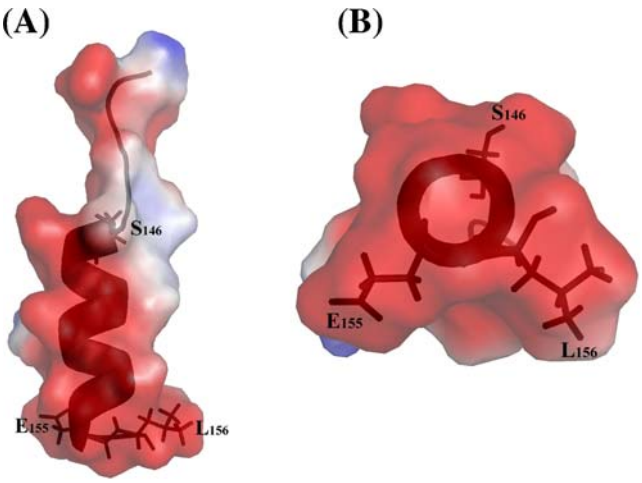

Fig. 8 Side view (**a**) and bottom view from the C-terminal (**b**) of $b_{140–156}$ showing the triangular arrangement of residues Ser_{146}, Glu_{155} and Leu_{156} in the electrostatic potential surface of the peptide, drawn in *pyMol* (DeLano 2001)

segment (Altendorf et al. 2000; Stalz et al. 2003), by the residues between 80 and 109 of subunit *b*, which are in neighbourhood to the major subunit α and β (Vogel 2000; McLachlin et al. 2000), and the C-terminus of *b*, likely through C-terminus of subunit δ (Rodgers et al. 1997; McLachlin et al. 2000). The so-called δ-binding domain of *b* includes the amino acids 120 to 156 (Dunn et al. 2000). The presented FCS titration data demonstrate that the association of subunit δ and *b* occurs via the very C-terminal peptide sequence of $b_{140–156}$ and the C-terminal segment $\delta_{91–177}$. The binding affinity determined for the binding of $b_{140–156}$ to $\delta_{91–177}$ is comparable to values of ≥2 and 5–10 μM of $b_{25–156}$ to δ-binding as determined by NMR spectroscopy (Rodgers et al. 1997) and analytical ultracentrifugation (Dunn and Chandler 1998), respectively. Removal of four residues from the C-terminus of *b* disrupts binding of δ and abolishes proton translocation of the enzyme (Takeyama et al. 1988). Moreover, crosslinking data in which a Cys at position 146 (mutant *b* Ser146Cys) forms a disulfide product with δ shows the importance of the very C-terminus in *b*–δ assembly (Rodgers et al. 1997). A chemical crosslink could also be described in the Glu155Cys and Met158Cys mutant of subunit *b* and δ, respectively, using a bifunctional crosslinker of about 1.1 nm in length (McLachlin et al. 2000). Previously, a Leu156Cys mutant of subunit *b* has been generated and crosslinking between this cysteine and the endogenous Cys_{90} of the α subunit has been observed, using $CuCl_2$ as oxidizing agent (Rodgers and Capaldi 1998). The novel 3D structure of $b_{140–156}$ shows a short flexible N-terminal tail (residues 140–145) followed by an α-helix, formed by the residues 146–156 (Fig. 7). The charge distribution of the peptide is amphiphilic, with the negative charge spread on one side from the N- to the C-terminal end of the structure while the positive charge and a hydrophobic surface form sides of the helix region. The residue Ser_{146} is a part of the hydrophobic area, made-up by the residues $Ileu_{147}$, Val_{148}, Leu_{151}, Val_{152} and Leu_{156}, which might be favorable to form hydrophobic interactions with the C-terminal part of δ. In contrast, the residue Glu_{155} is located on the opposite and negatively charged surface site of the helix. Therefore, the crosslink product between *b*E155C and δM158C could only be generated by the bifunctional crosslinker and explains the relatively low crosslink yield (McLachlin et al. 2000). Moreover, replacements of Glu_{155} by Asp, Gln, Lys or Ala of subunit *b* did not alter the binding to the F_1 sector (Takeyama et al. 1988), which is in line with the orientation of the hydrophobic area facing the binding site to subunit δ. The presented solution structure of $b_{140–156}$ shines light to the disulfide bond between *b*L156C and α Cys_{90} (Rodgers and Capaldi 1998). Leu_{156}, which together with Ser_{146} and Glu_{155} have a triangular arrangement inside the α-helix, is located at the very end of *b*, and becomes accessible for residue α Cys_{90}, which is within the N-terminal β-barrel domain of α, and shown to be implicated in the binding of δ (Ogilvie et al. 1997; Fig. 8).

In summary, the data presented demonstrate that the peripheral stalk domain $b_{22–156}$ of the *E. coli* subunit *b* exists in a boomerang-like shape in solution. The similarity in shape with the mitochondrial F_1F_O ATP synthase *b* subunit and the related H subunit of the A_1A_O ATP synthase is in line with their statical and mechanistical properties inside these classes of enzymes. Furthermore, the 3D structure of $b_{140–156}$ in solution provides the structural basis towards a more complete understanding of the interaction of subunit *b*, δ and α inside the enzyme.

Acknowledgment This research and the fellowships for R. Priya as well as for V. S. Tadwal were supported by a grant from the Ministry of Education, Singapore (ARC 6/06 and RG144/06). S. Gayen is a recipient of the Graduate Research Scholarship, Nanyang Technological University, Singapore.

References

Altendorf K, Stalz W, Greie J, Deckers-Hebestreit G (2000) J Exp Biol 203:19–28
Andrade MA, Chacon P, Merelo JJ, Moran F (1993) Protein Eng 6:383–390
Bhatt D, Cole SP, Grabar TB, Claggett SB, Cain BD (2005) J Bioenerg Biomembr 37:67–74
Biuković G, Rössle M, Gayen S, Mu Y, Grüber G (2007) Biochemistry 46:2070–2078
Böhm G (1992) Protein Eng 5:191–195
Boulin CJ, Kempf R, Koch MHJ, McLaughlin SM (1986) Nucl Instrum Methods A 249:399–407
Boulin CJ, Kempf R, Gabriel A, Koch MHJ (1988) Nucl Instrum Methods A 269:312–320
Brusilow WSA, Scarpetta MA, Hawthorne CA, Clark WP (1989) J Biol Chem 264:1528–1533
Capaldi RA, Aggeler R, Wilkens S, Grüber G (1996) J Bioenerg Biomembr 28:397–402
Del Rizzo PA, Bi Y, Dunn SD, Shilton BH (2002) Biochemistry 41:6875–6884
Del Rizzo PA, Bi Y, Dunn SD (2006) J Mol Biol 364:735–746
DeLano WL (2001) The pyMol molecular graphics system. DeLano Scientific, San Carlos, CA
Deléage G, Geourjon C (1993) Comp Appl Biosci 9:197–199
Dickson VK, Silvester JA, Fearnley IM, Leslie AGW, Walker JE (2006) EMBO J 25:2911–2918
Dmitriev O, Jones PC, Jiang W, Fillingame RH (1999) J Biol Chem 274:15598–15604
Dunn SD, Chandler J (1998) J Biol Chem 273:8646–8651
Dunn SD, Revington M, Cipriano DJ, Shilton BH (2000) J Bioenerg Biomembr 32:347–355
Grüber G (2000) J Bioenerg Biomembr 32:341–346
Grüber G, Hausrath A, Sagermann M, Capaldi RA (1997) FEBS Lett 410:165–168
Grüber G, Godovac-Zimmermann J, Link TA, Coskun Ü, Rizzo VF, Betz C, Bailer S (2002) Biochem Biophys Res Commun 298:383–391
Guinier A, Fournet G (1955) Small angle scattering of X-rays. Wiley, New York

Hausrath AC, Grüber G, Matthews BW, Capaldi RA (1999) Proc Natl Acad Sci USA 96:13697–13702
Herrmann T, Güntert P, Wüthrich K (2002) J Mol Biol 319:209–227
Hornung T, Volkov OA, Zaida TMA, Delannoy S, Wise JG, Vogel PD (2008) Biophys J 94:5053–5064
Hunke C, Chen WJ, Schäfer HJ, Grüber G (2007) Protein Expr Purif 53:378–383
Jemilawon J, Awuah Asiamah I, Bernstein HJ, Darakev G, Darakev N, Kamburov P (2007) Use of CBFlib for map support. In: Poster presentation at poster session B, Proceedings of the 9th International Conference on Biology and Synchrotron Radiation (BSR 2007), 13–17 August 2007, Manchester, UK
Keis S, Kaim G, Dimroth P, Cook GM (2004) Biochm Biophys Acta 1676:112–117
Kneller DG, Goddard TD (1997) SPARKY 3.105 edit. University of California, San Francisco, CA
Konarev PV, Volkov VV, Sokolova AV, Koch MHJ, Svergun DI (2003) J Appl Crystallogr 36:1277–1282
Laemmli UK (1970) Nature 227:680–685
Manavalan P, Johnson WC Jr (1987) Anal Biochem 167:76–85
McLachlin DT, Dunn SD (2000) Biochemistry 39:3486–3490
McLachlin DT, Coveny AM, Clark SM, Dunn SD (2000) J Biol Chem 275:17571–17577
Ogilvie I, Aggeler R, Capaldi RA (1997) J Biol Chem 272:16652–16656
Pedersen PL, Ko YH, Hong S (2000) J Bioenerg Biomembr 32:325–332
Petoukhov MV, Konarev PV, KiKhney AG, Svergun DI (2007) J Appl Cryst 40:223–228
Provencher SW (1982) Comput Phys Commun 27:213–227
Revington M, Dunn SD, Shaw GS (2002) Protein Sci 11:1227–1238
Rodgers AJW, Capaldi RA (1998) J Biol Chem 273:29406–29410
Rodgers AJ, Wilkens S, Aggeler R, Morris MB, Howitt SM, Capaldi RA (1997) J Biol Chem 272:31058–31064
Sreerama N, Woody RW (1993) Anal Biochem 209:32–44
Stalz W, Greie J, Deckers-Hebestreit G, Altendorf K (2003) J Biol Chem 278:27068–27071
Svergun DI (1992) J Appl Crystallogr 25:495–503
Svergun DI (1993) J Appl Crystallogr 26:258–267
Svergun DI (1997) J Appl Crystallogr 30:792–797
Svergun DI, Petoukhov MV, Koch MHJ (2001) Biophys J 80:2946–2953
Takeyama M, Noumi T, Maeda M, Futai M (1988) J Biol Chem 263:16106–16112
Vogel PD (2000) J Bioenerg Biomembr 32:413–421
Weber J (2006) Biochim Biophys Acta 1757:1162–1170
Wilkens S (2000) J Bioenerg Biomembr 32:333–340
Wilkens S, Dunn SD, Chandler J, Dahlquist FW, Capaldi RA (1997) Nat Struct Biol 4:198–201
Wise JG, Vogel PD (2008) Biophys J 94:5040–5052
Wood KS, Dunn SD (2007) J Biol Chem 282:31920–31927
Wüthrich K (1986) NMR of proteins and nucleic acids. Wiley, New York